

FASTER: TOWARD EFFICIENT AUTOREGRESSIVE VISION LANGUAGE ACTION MODELING VIA NEURAL ACTION TOKENIZATION

Yicheng Liu^{1,4§*}, Shiduo Zhang^{2,3§*}, Zibin Dong^{1,5*}, Baijun Ye^{1*}, Tianyuan Yuan^{1,4}, Xiaopeng Yu^{2,3}, Linqi Yin^{2,3}, Chenhao Lu^{1,4}, Junhao Shi^{2,3}, Luca Jiang-Tao Yu⁶, Liangtao Zheng⁷, Tao Jiang⁴, Jingjing Gong^{3†}, Xipeng Qiu^{2,3†}, Hang Zhao^{1,4†}

¹Tsinghua University, ²Fudan University, ³Shanghai Innovation Institute, ⁴Galaxea AI
⁵Tianjin University, ⁶Hong Kong University, ⁷UCSD

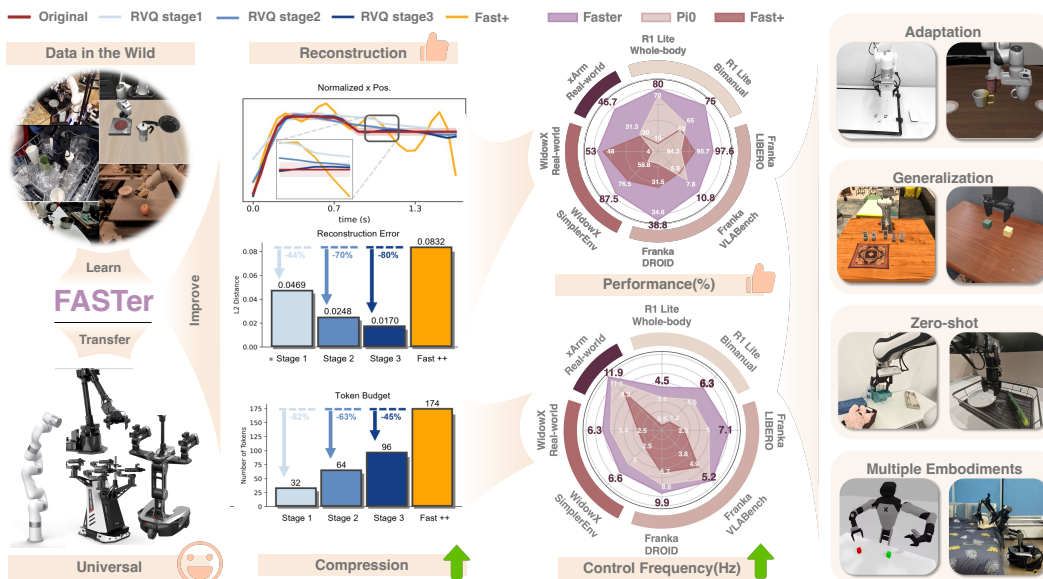


Figure 1: **FASTer** combines a learnable action tokenizer (FASTerVQ) and an autoregressive VLA model (FASTerVLA), achieving efficient compression, fast control, and strong performance across eight real and simulated embodiments.

ABSTRACT

Autoregressive vision-language-action (VLA) models have recently demonstrated strong capabilities in robotic manipulation. However, their core process of action tokenization often involves a trade-off between reconstruction fidelity and inference efficiency. We introduce **FASTer**, a unified framework for efficient and generalizable robot learning that integrates a learnable tokenizer with an autoregressive policy built upon it. FASTerVQ encodes action chunks as single-channel images, capturing global spatio-temporal dependencies while maintaining a high compression ratio. FASTerVLA builds on this tokenizer with block-wise autoregressive decoding and a lightweight action expert, achieving both faster inference and higher task performance. Extensive experiments across simulated and real-world benchmarks show that FASTerVQ delivers superior reconstruction quality, high token utilization, and strong cross-task and cross-embodiment generalization, while FASTerVLA further improves overall capability, surpassing previous state-of-the-art VLA models in both inference speed and task performance.

*Equal contribution. †Corresponding authors. §Project leaders.

{liuyicheng23@mails, hangzhao@mail}.tsinghua.edu.cn

{sdzhang23@m, xpqiu@}.fudan.edu.cn, jjgong@sii.edu.cn

1 INTRODUCTION

Vision-Language-Action (VLA) models represent a paradigm shift in robotics, embodying generalist robot policies trained on increasingly large-scale robotic datasets (Chenjia Bai, 2024). These models are categorized primarily by their method of robot action prediction, with the most prominent approaches being diffusion-based (Team et al., 2024; Black et al., 2024) and autoregressive VLA (Belkhale & Sadigh, 2024; Kim et al., 2024; Pertsch et al., 2025; Zhou et al., 2025) models. While diffusion-based models have demonstrated superior precision in manipulation tasks, they often exhibit a notable deficiency in leveraging critical visual and linguistic cues (Pertsch et al., 2025; Dong et al., 2025). In contrast, recent research indicates that a carefully designed autoregressive VLA model can increasingly bridge the performance gap with its diffusion-based counterparts, while simultaneously offering enhanced instruction-following capabilities (Pertsch et al., 2025; Intelligence et al., 2025; Hancock et al., 2025), superior scene generalization (Pertsch et al., 2025), and effective transfer of common-sense knowledge (Brohan et al., 2023). Most importantly, autoregressive VLA models share the most architectural similarity to the highly successful Vision-Language Models (VLMs), suggesting significant potential for future advancements.

A pivotal challenge within autoregressive VLA models is the development of an appropriate tokenization scheme to discretize continuous robot action sequence into action tokens (Wang et al., 2025c; Pertsch et al., 2025). Numerous sequence modeling studies, including LLMs and Speech-LLMs, have demonstrated that tokenizer quality directly determines model performance (Radford et al., 2019; Zhang et al., 2023; Gong et al., 2025). A further challenge for autoregressive VLA models is their inference efficiency, as they are considerably slower than diffusion-based counterparts (Kim et al., 2024; Intelligence et al., 2025). From this perspective, an effective action tokenization method must fulfill four key requirements: i) **High compression efficiency**: It must generate a minimal number of tokens for long sequences to ensure efficient and fast inference. ii) **Robust reconstruction quality**: As fewer tokens reduce the available information space, it is essential to guarantee high reconstruction fidelity rather than pursuing compression at the expense of accuracy. iii) **2D structural modeling**: the tokenizer must account for the two-dimensional nature of action sequences—comprising both the *action dimension*, where each component carries distinct physical semantics with limited redundancy, and the *temporal (horizon) dimension*, which often exhibits substantial redundancy across time. Modeling these coupled structures jointly is essential to achieve a favorable trade-off between efficiency and accuracy. iv) **Flexibility**: The tokenizer should enable out-of-the-box applicability across different backbones, tasks, and embodiments, thereby serving as a measure of its generalization ability. However, our preliminary experimental results, as illustrated in Figure 1, indicate that existing tokenization methods fail to comprehensively satisfy these principles.

To address these challenges, we introduce **FASTer (Flexible Action Sequence Tokenization for efficient inference)**, a unified framework consisting of two complementary components: **FASTerVQ** and **FASTerVLA**. **FASTerVQ** first non-uniformly groups the action sequence into semantically meaningful patches, effectively mitigating the imbalance of data distribution across different action dimensions. A hybrid transformer encoder is then employed to extract latent representations, which are subsequently quantized via residual vector quantization (RVQ) (Parker et al., 2025; Lee et al., 2022). This design achieves a superior balance between reconstruction fidelity and compression ratio—preserving fine-grained motion details even under a significantly smaller token budget. The tokenizer is trained to reconstruct actions in both temporal and frequency domains, enabling it to capture local dynamics and global trends simultaneously. Pretrained on large-scale robot datasets, **FASTerVQ** exhibits strong generalization across embodiments and tasks, achieving extremely high compression rates while maintaining near-lossless reconstruction, even for high-dimensional control such as whole-body coordination. Building upon **FASTerVQ**, **FASTerVLA** employs block-wise autoregressive decoding that leverages the structured latent space and the partial independence of tokens along the action dimension, enabling efficient parallel prediction within each block while maintaining coherent spatio-temporal structure. Furthermore, a lightweight action expert, architecturally aligned with the VLM backbone yet highly parameter-efficient, is introduced to bridge the modality gap between linguistic reasoning and continuous control. Together, these innovations allow **FASTerVLA** to achieve faster and more stable inference, stronger multimodal alignment, and consistent state-of-the-art performance across diverse tasks, embodiments, and model scales. Our contributions are summarized as follows:

- We propose **FASTerVQ**, a compact and high-compression-ratio action tokenizer that combines transformer-based residual vector quantization (RVQ) with a lightweight mixture mechanism. This design jointly compresses action sequences into a unified discrete codebook while preserving control-relevant structure, enabling downstream VLAs to more effectively leverage its outputs for action reasoning and generation.
- We introduce block-wise autoregressive decoding for efficient action-token modeling, together with a share structured action expert that aligns with the VLM backbone. These components jointly unleash the capability of autoregressive VLAs, allowing them to achieve faster inference while maintaining high accuracy.
- We establish a comprehensive benchmark covering four real robots and four simulated environments, providing the first systematic analysis of action tokenization for VLAs. Extensive experiments demonstrate that **FASTerVQ** achieves superior trade-offs between reconstruction fidelity and code length, and that **FASTerVLA** consistently delivers state-of-the-art performance across embodiments, tasks, and VLM backbones in both simulated and real-world settings.

2 RELATED WORK

Vision-Language-Action models. With advances in LLMs and multimodal systems (Sun et al., 2024; Achiam et al., 2023; Bai et al., 2023; Dubey et al., 2024), Vision-Language-Action (VLA) models have emerged as a promising direction for universal manipulation, leveraging the scalability of pretrained VLMs (Brohan et al., 2023; Driess et al., 2023; Kim et al., 2024; Black et al., 2024; Pertsch et al., 2025; Intelligence et al., 2025). Continuous control is typically modeled through either diffusion-based methods (Bjorck et al., 2025; Black et al., 2024; Kim et al., 2025) or autoregressive prediction over discretized actions (Brohan et al., 2023; Kim et al., 2024; Pertsch et al., 2025). Although autoregressive VLAs offer strong language grounding and generalization, they remain slower than non-autoregressive approaches (Brohan et al., 2023; Pertsch et al., 2025; Black et al., 2024). Our method instead learns a compact, structured discrete action space that aligns with pretrained VLMs, allowing autoregressive policies to operate at a more efficient token granularity and bringing inference speed into a practically usable regime.

VQ Tokenizer. VQ tokenization is widely used for modal compression across images (Yu et al., 2024; Sargent et al., 2025; Tian et al., 2024; Bao et al., 2022), video (Yu et al., 2023; Tang et al., 2024; Zhao et al., 2024; Wang et al., 2024a), audio (Casanova et al., 2024; Parker et al., 2025; Zhang et al., 2023; Lahrichi et al., 2025), graphs (Wang et al., 2025a; Zeng et al., 2025; Nguyen et al., 2024), and multimodal fusion (Sadok et al., 2025; Liu et al., 2025; Wang et al., 2024b). Audio codecs and action tokenizers share key traits: both process continuous time-series with short-term fluctuations, long-term trends, and periodic patterns (Parker et al., 2025; Zhai et al., 2025); both face non-uniform information density (Parker et al., 2025; Zhang et al., 2023); and both require strong temporal causality to ensure sequence coherence (Lahrichi et al., 2025). FASTerVQ therefore adopts an audio-inspired residual architecture, and our experiments confirm that, with sufficient data, such VQ designs inherit the strong generalization and scaling behavior observed across modalities.

Action tokenization. Autoregressive VLAs require discretizing continuous actions. Early approaches serialize each action dimension (Brohan et al., 2023; Kim et al., 2024), while later methods flatten full action chunks into 1D sequences (Zhao et al., 2023; Chi et al., 2024; Pertsch et al., 2025; Belkhale & Sadigh, 2024) using relative (Black et al., 2024; Intelligence et al., 2025) or delta actions (Pertsch et al., 2025). Existing tokenizers—binning (Brohan et al., 2023; Kim et al., 2024), DCT+BPE (Pertsch et al., 2025), and VQ variants (Belkhale & Sadigh, 2024; Wang et al., 2025c)—either under-compress, over-fragment, or lack reconstruction fidelity, producing action vocabularies that remain challenging for AR VLAs to model.

Block-wise generation. Chunk-wise generation appears across modalities: long-video models synthesize segments sequentially, conditioning each chunk on the last frame of the previous one (Zhang & Lim, 2024; Yang et al., 2025b), speech models adopt dynamic chunk-wise prediction for faster autoregressive synthesis (Li et al., 2025), and language models explore multi-token decoding or block-wise diffusion to reduce sequential depth (Li et al., 2024b; Arriola et al., 2025). In robot control, chunk policies (Zhao et al., 2023) are induced to mitigate compounding error, while (Zhang et al., 2025) show that chunked causal transformers further reduce autoregressive steps. (Kim et al., 2025) also performs parallel chunk decoding. Our approach instead performs block-wise autoregression over discrete action codes, enabling fast multi-token prediction while preserving AR consistency.

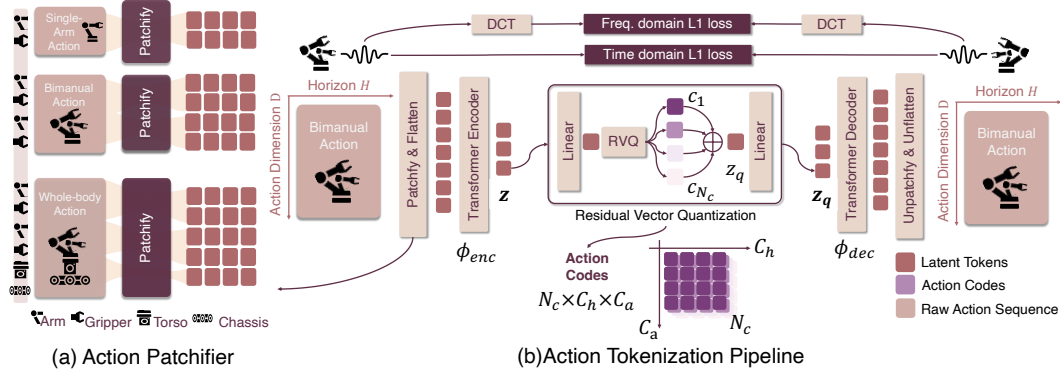


Figure 2: **FASTerVQ**. (a) The raw action sequence is patchified into compact tokens based on their embodied configuration. (b) **FASTerVQ** applies DCT and L1 reconstruction losses and adopts RVQ, encoding actions into N_c code levels; each level can be reshaped into a $C_h \times C_a$ tensor.

3 METHOD

Problem Formulation. We consider the problem of learning a VLA policy that maps multimodal observations to sequences of robot actions. At each time step, the policy receives three inputs: an RGB image $I_t \in \mathbb{R}^{H \times W \times 3}$, a proprioceptive state $s_t \in \mathbb{R}^{d_s}$, and a language instruction $l \in \mathcal{L}$. The output is an action sequence of horizon length H , denoted as $A_{t:t+H} = (a_t, a_{t+1}, \dots, a_{t+H-1})$. Instead of predicting continuous actions directly, we represent each action chunk as a sequence of discrete codes (z_1, \dots, z_N) obtained via a VQ tokenizer. The policy is then trained in an autoregressive manner to generate these codes conditioned on (I_t, s_t, l) . The VQ tokenizer subsequently decodes the generated codes back into continuous actions.

A key bottleneck of autoregressive VLA models lies in the token sequence length. Since tokens are generated sequentially, each requiring a full forward pass through a large transformer, inference latency grows quadratically due to attention complexity with respect to sequence length. Moreover, correct decoding requires all tokens to be predicted accurately, making the model brittle when token lengths vary. This issue is particularly acute in whole-body control, where high degrees of freedom lead to long action sequences. For example, the FAST tokenizer requires 150–200 tokens to represent a 2-second motion, which corresponds to an inference delay of roughly three seconds. Our experiments with policies initialized from multiple VLMs further confirm that training a VLA on variable-length codes is substantially more challenging than on fixed-length representations. To overcome these limitations, we propose **FASTerVQ** and **FASTerVLA**, which compress action representations, reduce the effective autoregressive depth, and equip the policy with a lightweight expert pathway attuned to action-level structure. The next sections unfold these components in detail.

3.1 FASTerVQ

Our action tokenizer architecture comprises two main components: an **action patchifier** and a transformer-based **Residual Vector Quantization (RVQ) Tokenizer**. This design leverages the unique characteristics of robotic action sequences to enhance tokenization efficiency and fidelity.

Action Patchifier. Although robot action sequences could be fed directly into a transformer as a sequential vector, a preliminary patching step proves to be more effective due to two key properties of these sequences. First, robot actions often exhibit smoothness and temporal redundancy, which can be addressed by chunk-wise grouping. This approach increases both the compression rate and the information density per token. Second, the different dimensions of an action vector correspond to distinct physical quantities with highly non-uniform data distributions. For instance, a robot’s gripper state is often binary (open or closed), and the base movement is typically zero during arm manipulation. This distributional imbalance can pose training challenges. Grouping similar physical quantities a priori effectively mitigates this issue. Specifically, for an action sequence $A_{t:t+H} = (\mathbf{a}_t, \mathbf{a}_{t+1}, \dots, \mathbf{a}_{t+H-1})$, where $\mathbf{a}_t \in \mathbb{R}^D$, we perform a two-dimensional partitioning. The temporal dimension is uniformly divided into m groups of length h . And the action dimensions are non-uniformly partitioned into n groups based on their physical characteristic (e.g., end-effector position, orientation, and gripper state are grouped separately). Each group is then padded to the largest group, d . This process yields a structured tensor of shape $(m \cdot h) \times (n \cdot d)$, which is subsequently flattened into a set of patches, $\mathbf{a}_{t:t+H}^P \in \mathbb{R}^{(m \cdot n) \times (h \cdot d)}$. This procedure can be conceptualized as a form of

non-overlapping convolution, a method widely adopted for early data processing in various domains due to its proven efficacy (Yu et al., 2023; Liu et al., 2023b).

Residual VQ Action Tokenizer. Inspired by the success of Residual Vector Quantization (RVQ) and transformer-based codecs (Parker et al., 2024), we design a transformer-based hybrid encoder–decoder architecture named Transformer Action AutoEncoder (TAAE). It combines the adaptive global receptive field of a transformer and the local relation modeling and downsampling capacity of convolutions, forming an effective information bottleneck. Moreover, RVQ naturally imparts a **coarse-to-fine** structure: early stages capture low-frequency components, while later stages refine high-frequency residuals. This property not only improves representational efficiency but also stabilizes both the training and inference of downstream VLA models. For an input action patch $\mathbf{a}_{t:t+H}^P$, the encoder ϕ_{enc} downsamples it into a latent embedding $\mathbf{z} \in \mathbb{R}^{C_h \times C_a}$. We then apply RVQ with N_c quantization levels, decomposing \mathbf{z} into residuals as $\mathbf{r}_1 = \mathbf{z}$, $\mathbf{r}_{i+1} = \mathbf{r}_i - \mathcal{Q}_i(\mathbf{r}_i)$, and the quantized latent embedding is $\mathbf{z}_q = \sum_{i=1}^{N_c} \mathcal{Q}_i(\mathbf{r}_i)$. Each quantizer \mathcal{Q}_i selects its nearest codebook entry e_k with index $k = \arg \min_j \|\mathbf{r}_i - e_j\|^2$. Collecting these indices yields a discrete code tensor $C \in \{1, \dots, |\mathcal{Z}|\}^{N_c \times C_h \times C_a}$, where each element $c_{i,h,a}$ denotes the index of the chosen codebook vector at stage i and location (h, a) . This tensor C serves as the action tokens for the downstream policy. The quantized embedding \mathbf{z}_q is then passed through the decoder ϕ_{dec} via a straight-through estimator (STE) (Van Den Oord et al., 2017) to reconstruct the action patch $\hat{\mathbf{a}}_{t:t+H}^P$.

Training Objective. The action tokenizer is trained by minimizing the reconstruction loss \mathcal{L}_{rec} and the commitment loss \mathcal{L}_{commit} . The reconstruction loss \mathcal{L}_{rec} is composed of two components: an ℓ_1 loss on the temporal action signal $\mathbf{a}_{t:t+H}^P$ for step-wise action reconstruction, and an ℓ_1 loss on the Discrete Cosine Transform (DCT) of the signal, $\text{DCT}(\mathbf{a}_{t:t+H}^P)$, to capture the overall trend. We select the ℓ_1 loss due to its robustness against the extreme value noise often present in real-world robot action data, which contributes to training stability:

$$\mathcal{L} = \|\mathbf{a}_{t:t+H} - \hat{\mathbf{a}}_{t:t+H}\|_1 + \|\text{DCT}(\mathbf{a}_{t:t+H}) - \text{DCT}(\hat{\mathbf{a}}_{t:t+H})\|_1 + \lambda \cdot \|\mathbf{z} - \text{sg}(\mathbf{z}_q)\|_2^2, \quad (1)$$

where sg denotes the stop-gradient operation, and λ balances the loss components. The RVQ codebooks are updated using an exponential moving average (EMA) with dead codes reinitializing.

3.2 FASTERVLA

Architecture. As shown in Figure 3 (a), FASTerVLA follows most VLM structure—a vision tower, a projection layer, and a transformer-based language backbone—to ensure compatibility with standard pretrained checkpoints. Visual inputs are encoded by the vision tower and projected into the model dimension; language instruction follows the usual text pipeline. *Action embeddings & Proprioception encoding:* We resize the original embedding table to include $|C|$ new slots for action codes. Proprioceptive states are discretized into integers and tokenized as text. *Positional encoding and spacing augmentation:* We adopt rotary position embeddings (RoPE) for positional encoding. Since actions are encoded at a fixed sequence length, naively predicting a fixed-length target can lead to position overfitting. To mitigate this, we apply spacing augmentation: during training, the relative offset between adjacent action tokens is perturbed around unit spacing, i.e., if p_i denotes the position of token i , we set $p_i = p_{i-1} + 1 + \epsilon_i$, where ϵ_i is a small integer jitter uniformly sampled from $\mathcal{U}[0, k]$ (e.g., $k = 2$), while preserving token order. At inference, we revert to a fixed spacing (e.g., $p_i = p_{i-1} + 2$). This encourages the model to rely on content rather than absolute positions within the horizon. *Lightweight action expert:* Inspired by π_0 (Black et al., 2024), we add a lightweight action expert sharing the backbone architecture but with fewer parameters. The backbone encodes the multimodal context once, while the expert autoregressively decodes action tokens from these

Algorithm 1 FASTer Tokenizer

Require: FASTerVQ quantizers $\{\mathcal{Q}_i\}_{i=1}^{N_c}$, encoder ϕ_{enc} and decoder ϕ_{dec} .

procedure ENCODE($a_{t:t+H}$)

$r \leftarrow z \leftarrow \phi_{enc}(\text{Patchify}(a_{t:t+H}))$

$C \leftarrow [], z_q \leftarrow 0$

for $i = 1$ to N_c **do**

$z_q += \mathcal{Q}_i(r), r -= \mathcal{Q}_i(r)$

$C.append(c_i)$

return C

procedure DECODE(C)

$z_q \leftarrow 0$

for $i = 1$ to N_c **do**

$z_q += \mathcal{Q}_i.lookup(C[i])$

$a_{t:t+H} \leftarrow \text{UnPatchify}(\phi_{dec}(z_q))$

return $a_{t:t+H}$

procedure VQ_TRAINING($a_{t:t+H}$)

$\hat{a}_{t:t+H} = \text{DECODE}(\text{ENCODE}(a_{t:t+H}))$

Train with the loss \mathcal{L} in Equation (1)

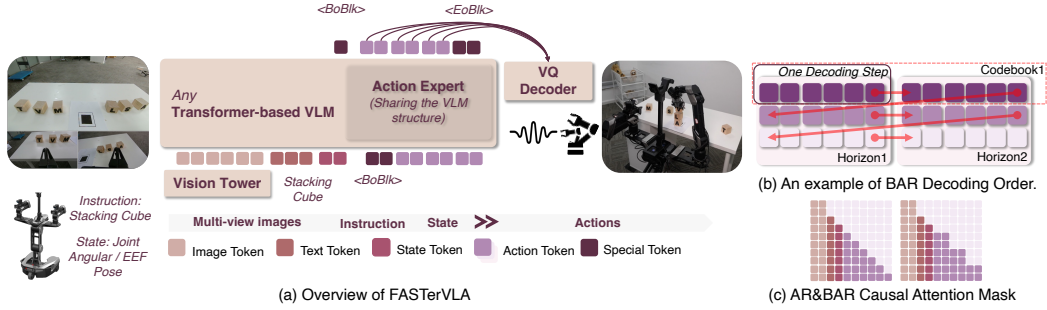


Figure 3: **FASTerVLA**. (a) The model takes RGB images, proprioceptive states, and a language instruction as inputs to a transformer-based VLM. An Action Expert autoregressively generates discrete action tokens, which a VQ decoder maps into the final continuous action sequence. (b) Codes are generated codebook-wise before advancing along the temporal horizon, yielding greater stability than horizon-first decoding (red arrows denote the decoding order). (c) Left: vanilla causal mask; Right: Block-wise causal mask, where tokens within each block attend to preceding and intra-block tokens. Token colors denote different modalities.

features. This design mitigates interference with pretrained weights while enabling lightweight and efficient decoding.

Block-wise Autoregression (BAR). In the vanilla setting, the policy is trained autoregressively with a next-token prediction objective under teacher forcing:

$$\mathcal{L}_{\text{AR}} = - \sum_{i=1}^N \log p_{\theta}(c_i | c_{<i}, I_t, s_t, x), \quad (2)$$

where $C = (c_1, \dots, c_N)$ denotes the sequence of discrete action codes produced by the VQ tokenizer, and $N = N_c \times C_h \times C_a$ is the total number of tokens per action chunk. At inference, tokens are generated sequentially until the $\langle \text{eos} \rangle$ symbol, and decoded by the VQ decoder into a continuous trajectory $A_{t:t+H}$.

A key inefficiency of vanilla AR arises because many action codes are only weakly coupled across dimensions: distinct action dimensions often carry independent physical semantics and heterogeneous distributions. To address this, we adopt a block-wise objective that predicts the next block of tokens in a single forward pass. Specifically, we partition C into J contiguous blocks of size B , i.e., $C = \{C_1, \dots, C_J\}$ with $C_j = (c_{j,1}, \dots, c_{j,B})$ and $N = JB$. Training still uses teacher forcing, and the BAR loss is defined as

$$\mathcal{L}_{\text{BAR}} = - \sum_{j=1}^J \sum_{i=1}^B \log p_{\theta}(c_{j,i} | C_{<j}, I_t, s_t, x). \quad (3)$$

We replace the standard causal mask with a block-wise causal mask that allows intra-block attention (Fig. 3c). To integrate text and action generation, BAR uses two control tokens, $\langle \text{BoBlk} \rangle$ and $\langle \text{EoBlk} \rangle$, to toggle between block-wise and standard AR prediction, enabling seamless switching within a single sequence. In practice, when the model outputs $\langle \text{BoBlk} \rangle$, this token is replicated B times and fed back as input to initiate prediction of the first block.

Decoding order. The VQ tokenizer outputs action codes arranged as a 3D tensor $C \in \mathbb{Z}^{N_c \times C_h \times C_a}$, spanning codebooks, temporal horizons, and action dimensions. FASTerVLA organizes decoding hierarchically across both the codebook and horizon dimensions (Fig. 3b). For each codebook, the model first decodes tokens along the horizon dimension $0, 1, \dots, C_h - 1$ before proceeding to the next codebook. This ordering aligns with the residual quantization pipeline, where earlier codebooks capture coarse, low-frequency components, and later ones refine higher-frequency residuals. Consequently, decoding progresses in a coarse-to-fine manner, improving representational efficiency and stabilizing both training and inference. Since each block is decoded in parallel, BAR reduces the number of forward passes from N to roughly N/B . As shown in Table 6, the number of blocks J is small (e.g., 3 on LIBERO), yielding up to a $3\times$ reduction in inference latency compared to π_0 (Black et al., 2024).

4 EXPERIMENTS

We comprehensively evaluate the proposed **FASTer** framework through a series of experiments covering both the tokenizer and the full VLA model. We first investigate **FASTerVQ** to understand its

Model	LIBERO					Simpler-Bridge				
	Spatial	Object	Goal	Long	Average	Spoon	Carrot	Block	Eggplant	Average
Diffusion Policy (Chi et al., 2023)	78.3	92.5	68.3	50.5	72.4	-	-	-	-	-
Octo-Base (Team et al., 2024)	78.9	85.7	84.6	51.1	75.1	12.5	8.3	0.0	43.1	16.0
SpatialVLA (Qu et al., 2025)	88.2	89.9	78.6	55.5	78.1	16.7	25.0	29.2	100.0	42.7
π_0 (Black et al., 2024)	96.8	98.8	95.8	85.2	94.2	66.7	58.3	58.3	88.3	66.7
π_{05} (Intelligence et al., 2025)	<u>98.8</u>	98.2	<u>98.0</u>	92.4	96.8	-	-	-	-	-
OpenVLA-OFT (Kim et al., 2025)	97.6	98.4	97.9	<u>94.5</u>	<u>97.1</u>	12.5	4.2	8.3	0.0	6.25
UniVLA (Bu et al., 2025)	96.5	96.8	95.6	92.0	95.2	54.2	66.7	50.0	4.2	43.8
OpenVLA (Kim et al., 2024)	84.7	88.4	79.2	53.7	76.5	32.0	30.0	18.0	38.0	29.5
Palligemma + Naive Tokenizer	55.8	64.8	64.4	31.2	54.1	66.7	29.2	12.5	54.2	40.9
MiniVLA (Belkhale & Sadigh, 2024)	-	-	-	77.0	-	68.0	44.0	70.0	14.0	49.0
VQ-VLA (Wang et al., 2025c)	-	-	75.2	60.0	-	12.5	8.0	6.0	0.0	6.3
π_0 FAST-R ¹ (Pertsch et al., 2025)	96.4	96.8	88.6	60.2	85.5	29.1	21.9	10.8	66.6	32.1
π_0 FAST-D (Pertsch et al., 2025)	96.6	97.2	96.0	86.8	94.2	77.5	<u>88.3</u>	68.3	71.7	76.5
FASTer w/o BAR	99.4	98.8	94.8	88.6	95.4	97.5	83.3	65.0	78.3	81.0
FASTer	98.0	99.4	98.6	95.4	97.9	<u>91.7</u>	93.3	<u>67.5</u>	<u>99.2</u>	87.9

Table 1: Policy performance on Libero and Simpler-Bridge benchmarks.

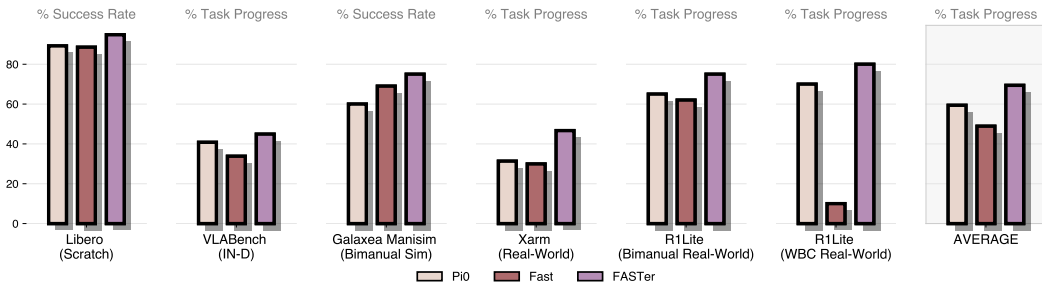


Figure 4: Policy performance across embodiments and environments. Results are reported in the in-distribution setting, covering two real-world embodiments and three simulated setups.

properties as an action tokenizer and then benchmark **FASTerVLA** across diverse tasks, embodiments, and backbones. Further ablation studies (4.4) analyze key design factors such as the tokenizer architecture and codebook size. These experiments aim to answer the following questions:

- 1) How well does **FASTerVQ** balance accuracy and efficiency in modeling action chunks? (4.2)
- 2) How flexible is **FASTer** across tasks, embodiments, and backbones? (4.2& 4.3)
- 3) How strong are the performance and generalization abilities of **FASTerVLA**? (4.3)
- 4) How do tokenizer performance and action code distributions affect overall VLA behavior? (4.3)

4.1 EXPERIMENT SETUPS

Benchmarks. We evaluate across nine benchmarks spanning five distinct embodiments in both simulated and real-world settings as illustrated in Figure 11. These tasks include deformable manipulation, whole-body control, instruction following, and long horizon manipulation. Details of the benchmarks and the setup of each task are provided in Appendix A.1.

Baselines. We begin by evaluating **FASTer** on the most widely used public benchmark, comparing it against prior state-of-the-art models spanning both non-autoregressive (top) and autoregressive (mid) architectures in Table 1. As other experiments’ baselines, we include π_0 (Black et al., 2024), a non-autoregressive VLA with flow matching, and π_0 -FAST (Pertsch et al., 2025), the state-of-the-art autoregressive VLA built on the FAST tokenizer.

Training. Unless otherwise specified, all baselines and **FASTerVLA** models in our experiments are initialized from checkpoints pretrained on large-scale robotics data (e.g., from π_0 -FAST). For Bridge and Droid experiments, all VLA models are instead initialized from pretrained VLM weights and pretrained on the same dataset to ensure a fair zero-shot evaluation. Detailed training configurations are provided in Appendix A.2.

¹ π_0 FAST-D: delta action chunks; π_0 FAST-R: relative action chunks. All results use π_0 FAST-D unless otherwise noted.

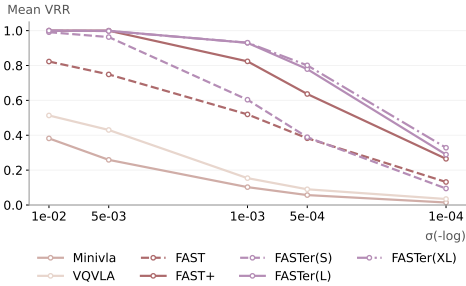


Figure 5: Average VRR of different action tokenizers under multiple error tolerances σ . FASTer achieves the best performance across all scales and exhibits clear data-scaling behavior.

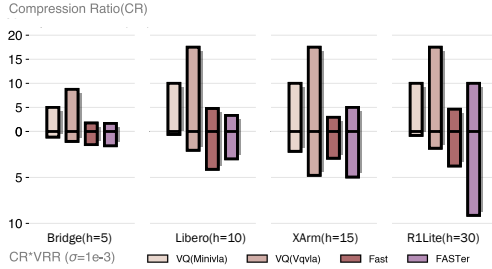


Figure 6: Compression rate vs. reconstruction trade-off across action horizons, where FASTer achieves the best balance, particularly for long sequences.

4.2 RESULTS AND ANALYSIS OF FASTERVQ

As introduced in Section 1, an effective action tokenizer should jointly achieve high reconstruction quality and high compression rate. Figure 5 and Figure 6 compares FASTer against Fast and other VQ tokenizers in terms of compression efficiency and reconstruction fidelity. During training, we observed that reconstruction loss alone often fails to capture meaningful action quality, as many low-level discrepancies correspond merely to motor or sensor noise rather than task-relevant deviations. In such cases, perfectly reconstructing noisy signals yields little practical benefit, since actions with minor deviations typically result in indistinguishable outcomes during real-world execution. To better capture functional fidelity, we introduce the **Valid Reconstruction Rate (VRR)**, which measures the proportion of reconstructed actions whose deviation from ground truth falls within a small tolerance threshold:

$$\text{VRR} = N_{\text{valid}}/N_{\text{total}}, \quad N_{\text{valid}} = \sum_{i=1}^{N_{\text{total}}} \mathbf{1}(\|\mathbf{a}_i^{\text{recon}} - \mathbf{a}_i^{\text{gt}}\|_1 < \sigma), \quad (4)$$

where N_{total} is the total number of actions, N_{valid} counts those within tolerance σ , $\mathbf{a}_i^{\text{recon}}$ and \mathbf{a}_i^{gt} denote reconstructed and ground-truth actions, $\mathbf{1}(\cdot)$ is the indicator function, and σ is a hyperparameter. For robot end-effector translation, σ corresponds to the Euclidean distance error measured in meters, whereas for end-effector rotation and joint positions, σ represents an angular error in radians. In practice, a reconstruction error on the order of 10^{-2} is sufficient to cause a noticeable degradation in task execution accuracy.

FASTerVQ Combines Compactness and Fidelity. In Figure 5 and Figure 6, while baseline VQ methods perform well in terms of compression ratio, they exhibit significant shortcomings in reconstruction accuracy—even on in-distribution datasets, as shown in Figure 13. As a result, the LLM backbone learns inherently erroneous action codes, which constrain overall performance, especially in high-precision tasks. In contrast, FASTerVQ achieves a favorable balance between compression and fidelity, preserving reconstruction accuracy while minimizing the number of tokens. Figure 6 further compares tokenizer performance across different control frequencies and sequence lengths. Thanks to its structured design, FASTerVQ maintains significantly higher compression efficiency on high-frequency action sequences.

FASTerVQ Efficiently Leverages Larger Data. A competent action tokenizer is expected to be capable of effectively scaling with large amounts of training data. To evaluate this property, we trained three variants of FASTerVQ on different amounts of data—FASTer(S), FASTer(L), FASTer(XL), and the details can be found in Table 3. As shown in Figure 5, FASTerVQ consistently delivers state-of-the-art reconstruction across multiple error tolerances σ , e.g., FASTerVQ(S) vs. FAST and FASTerVQ(L) vs. FAST+. This capability clearly exhibits a strong data-scaling trend. In particular, FASTerVQ-XL achieves nearly lossless action-chunk reconstruction at the physically meaningful tolerance level of $\sigma = 10^{-3}$, even when FASTerVQ is trained with data budgets that are equal to or smaller than those of FAST. Furthermore, our results confirm that FASTerVQ’s scaling behavior yields substantial gains in generalization—across tasks, embodiments and even action representations—demonstrated in Figure 8 and Figure 13. We will discuss this in detail in the following section.

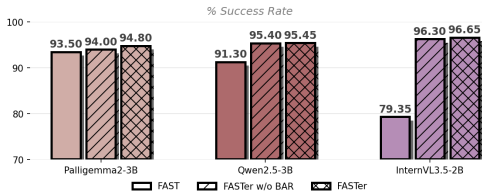


Figure 7: Comparison of FASTer, its non-BAR variant, and FAST across backbones on the Libero benchmark.

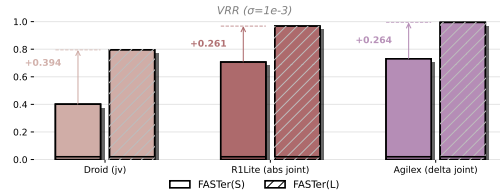


Figure 8: FASTer generalizes well across embodiments and action types with scaling trend.

FASTerVQ Generalizes Across Embodiments. We evaluate FASTerVQ’s generalization by training the tokenizer solely on single-arm delta-EEF trajectories, and testing it on tasks that differ in semantics, embodiment, and even action representation. For unseen tasks and embodiments, we test on our newly collected Widow and XArm datasets (Figure 13). For unseen action representations, we evaluate joint-velocity actions from Droid, absolute joint-position actions from Galaxea Open, and delta joint-position actions from Agilex (Figure 8). Across all settings, FASTerVQ maintains strong reconstruction performance, suggesting that action chunks from diverse robot platforms share a common structure once mapped into normalized action space. This indicates that FASTerVQ captures a transferable action prior and shows a clear data-scaling trend in both cross-embodiment and cross-action-type generalization.

4.3 RESULTS AND ANALYSIS OF FASTerVLA

In distribution Performance of FASTerVLA. We first evaluate the performance of FASTerVLA and several SOTA baselines in an in-distribution (ID) setting. This setting is characterized by using the same tasks and scenes as in the training set, but with randomized object layouts to ensure robustness. The evaluation is conducted across a comprehensive set of task suites, including three simulation environments: LIBERO, VLABench, and GalaxeaManisim, and three real-world robotic platforms: single-arm using xArm, the bimanual using R1Lite, and whole-body control using R1Lite (Figure 11). Our results (Table 1, Figure 4) show that FASTerVLA achieves a 97.9% success rate on the Libero benchmark, setting a new state of the art. Across all evaluated settings, it consistently outperforms prior baselines, with only a marginal gap to π_0 on VLABench. These findings highlight the strong potential of autoregressive VLAs—when equipped with an efficient tokenizer like FASTerVQ—to rival and even surpass diffusion-based approaches.

Out-of-Distribution Performance of FASTerVLA. To evaluate the generalization and robustness of FASTerVLA, we conduct tests in an out-of-distribution (OOD) setting where the training and evaluation tasks are distinct. This evaluation spans both simulation and real-world environments, including the VLABench suite and two physical platforms: WidowX (with VLAs pre-trained on BridgeData (Walke et al., 2023)) and Franka (pre-trained on DROID (Khazatsky et al., 2024)). In simulation, FASTerVLA achieves the highest overall success rate while exhibiting the lowest relative performance drop (29%) compared to its in-distribution baseline (Figure 9). On the real-world robotic platforms, it consistently outperforms prior baselines (Figure 10). In particular, on the Simpler-Bridge benchmark, FASTerVLA attains an 87.9% success rate, outperforming the second-best model by 12.9%, further demonstrating its superior generalization capability.

To better understand these results, we analyze the code distributions of different tokenizers on BridgeData (Table 8). Fast+ (57% of 2048) and FASTerVQ (100% of 4096) exhibit markedly higher codebook utilization than Fast (48% of 2048). Moreover, Fast shows a dominant token with $F_{\max} = 10\%$, while Fast+ and FASTerVQ achieve higher normalized entropy, indicating more balanced and information-rich token usage. Importantly, this balanced utilization translates into stronger task performance (Figure 10), where FASTerVLA and Fast+ achieve the highest task progress across zero-shot benchmarks such as *Bridge* and *Droid*. Overall, these findings suggest that diverse and evenly activated codebooks enhance action representation expressiveness, leading to better generalization and higher success rates.

Cross-backbone ability of FASTer. FASTer framework can also adapt to different backbones. We evaluated FASTerVLA with Palligemma (Steiner et al., 2024), Qwen2.5 (Yang et al., 2025a; Gao et al., 2025), and InternVL3.5 (Wang et al., 2025b) on the Libero benchmark (Figure 7). FASTer

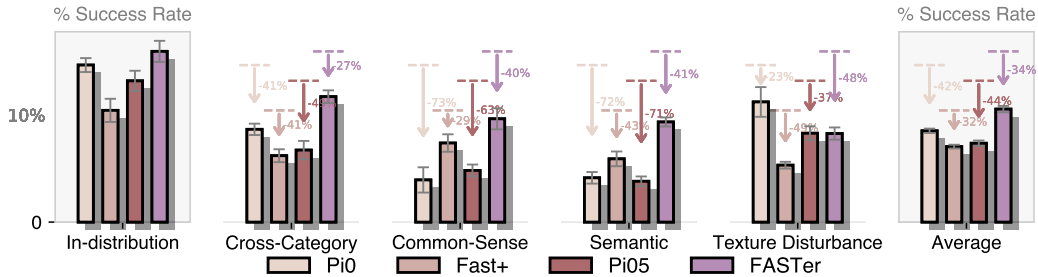


Figure 9: Evaluation results of generalization ability on VLABench. The evaluation dimensions cover generalization of language, vision, and goal and knowledge transfer.

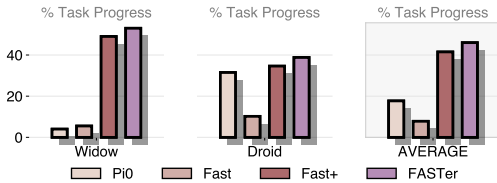


Figure 10: Comparison of zero-shot performance between FASTER and baselines on Droid and Bridge datasets.

model part	Time(Single)	Time(WBC)
image encoders	16 ms	23ms
observation forward pass	72 ms	105ms
AR forward pass	6.4*21 ms	-
BAR forward pass	7.4ms*3	8.51ms*12
FASTERVQ detokenization	2.7 ms	7ms
total inference	112ms	237ms

Table 2: The inference time is measured using a PyTorch implementation on an RTX 5090. WBC refers to a whole-body-control setting that uses an action DoF/chunk size of 21/32, whereas Single refers to a single-arm setting that uses 7/20.

consistently improved performance, most notably raising InternVL3.5-2B’s success rate by 17.3% to 96.65%, turning it from the weakest with FAST into the strongest overall. This gain stems from FASTER’s concise, regularized, and data-driven representation, which better matches instruction distributions and avoids the inefficiencies of variable-length tokens in FAST. The figure shows that FASTER’s improvement is driven primarily by its neural VQ tokenizer: swapping FAST for FASTERVQ yields most of the gain, with BAR adding only a smaller incremental boost. Additional results are reported in Section A.4.

Inference Efficiency of FASTER. We evaluate the inference efficiency of FASTER on an RTX 5090, using a PyTorch implementation across the LIBERO and R1Lite-WBC benchmarks. In the Single setting, the single-arm configuration in the LIBERO environment uses an action chunk size of 20 with two camera views; in the WBC setting, the 21-DoF configuration uses an action chunk size of 32 with three camera views. A detailed analysis is provided in Table 2. The results suggest that the dominant bottleneck lies in the observation encoding stage: both π_0 and our model spend approximately 88–127ms on this step. By comparison, the action tokenizer remains relatively light, contributing only about 2.7–7ms. We also test an AR version of FASTER to compare with BAR. Because BAR emits multiple tokens per forward pass, it can meaningfully reduce latency when a task requires a large number of action tokens. Under the same environment and computational setup described above, we further compare **FASTERVLA**, π_0 , and π_0 -FAST with a shared PaliGemma backbone in Table 5. On LIBERO, the runtimes are 112ms for **FASTERVLA**, 176ms for π_0 , and 197–556ms for π_0 -FAST. In the R1Lite-WBC tasks, where the action dimensionality is substantially larger, **FASTERVLA** and π_0 converge to similar runtimes (around 230ms), since **FASTERVLA** performs 12 forward passes. In contrast, π_0 -FAST incurs a significantly higher cost of 1,100–3,000ms, driven by the considerable number of action tokens required during decoding.

4.4 ADDITIONAL STUDIES

We ablate key design choices of **FASTERVQ** (tokenizer, codebook size, and residual depth) and **FASTERVLA** (action expert and block-wise decoding). The results confirm that the final configuration achieves the best balance of accuracy, efficiency, and stability. Detailed results and analysis are provided in Appendix A.3. Real-world rollouts of **FASTERVLA** are shown in Figure 15.

5 CONCLUSION

We propose an efficient autoregressive VLA framework that couples a flexible vector quantization module with a efficient VLA training inference setting. It delivers strong task performance with low-latency inference and generalizes across backbones, as the pretrained VQ can be reused in downstream tasks without retraining. The success stems from three key ideas: a codec-inspired RVQ balancing accuracy, diversity, and code length; block-wise autoregressive decoding for faster, expressive inference; and a lightweight mixture-of-experts VLA for action tokens. These results show that autoregressive modeling can be fast, transferable, and scalable for multimodal generation.

6 ETHICS STATEMENT

The authors have adhered to the ICLR Code of Ethics. This work does not involve human subjects, sensitive data, or raise any direct ethical concerns. All datasets used are publicly available.

7 REPRODUCIBILITY STATEMENT

We are committed to ensuring the reproducibility of our research. Our source code will be made public upon publication. Detailed descriptions of our methods and model architectures are available in the section 3. All experimental settings, including datasets, training hyperparameters, evaluation settings are specified in the section 4 and Appendix.

REFERENCES

- Josh Achiam, Steven Adler, Sandhini Agarwal, Lama Ahmad, Ilge Akkaya, Florencia Leoni Aleman, Diogo Almeida, Janko Altenschmidt, Sam Altman, Shyamal Anadkat, et al. Gpt-4 technical report. [arXiv preprint arXiv:2303.08774](#), 2023.
- Marianne Arriola, Aaron Gokaslan, Justin T Chiu, Zhihan Yang, Zhixuan Qi, Jiaqi Han, Subham Sekhar Sahoo, and Volodymyr Kuleshov. Block diffusion: Interpolating between autoregressive and diffusion language models. [arXiv preprint arXiv:2503.09573](#), 2025.
- Jinze Bai, Shuai Bai, Shusheng Yang, Shijie Wang, Sinan Tan, Peng Wang, Junyang Lin, Chang Zhou, and Jingren Zhou. Qwen-vl: A frontier large vision-language model with versatile abilities. [arXiv preprint arXiv:2308.12966](#), 2023.
- Hangbo Bao, Li Dong, Songhao Piao, and Furu Wei. BEit: BERT pre-training of image transformers. In [International Conference on Learning Representations, ICLR, 2022](#).
- Suneel Belkhale and Dorsa Sadigh. Minivla: A better vla with a smaller footprint, 2024. URL <https://github.com/Stanford-ILIAD/openvla-mini>.
- Johan Bjorck, Fernando Castañeda, Nikita Cherniadev, Xingye Da, Runyu Ding, Linxi Fan, Yu Fang, Dieter Fox, Fengyuan Hu, Spencer Huang, et al. Gr00t n1: An open foundation model for generalist humanoid robots. [arXiv preprint arXiv:2503.14734](#), 2025.
- Kevin Black, Noah Brown, Danny Driess, Adnan Esmail, Michael Equi, Chelsea Finn, Niccolo Fusai, Lachy Groom, Karol Hausman, Brian Ichter, et al. pi0: A vision-language-action flow model for general robot control. [arXiv preprint arXiv:2410.24164](#), 2024.
- Anthony Brohan, Noah Brown, Justice Carbajal, Yevgen Chebotar, Xi Chen, Krzysztof Chormanski, Tianli Ding, Danny Driess, Avinava Dubey, Chelsea Finn, Pete Florence, Chuyuan Fu, Montse Gonzalez Arenas, Keerthana Gopalakrishnan, Kehang Han, Karol Hausman, Alex Herzog, Jasmine Hsu, Brian Ichter, Alex Irpan, Nikhil Joshi, Ryan Julian, Dmitry Kalashnikov, Yuheng Kuang, Isabel Leal, Lisa Lee, Tsang-Wei Edward Lee, Sergey Levine, Yao Lu, Henryk Michalewski, Igor Mordatch, Karl Pertsch, Kanishka Rao, Krista Reymann, Michael Ryoo, Grecia Salazar, Pannag Sanketi, Pierre Sermanet, Jaspiar Singh, Anikait Singh, Radu Soricut, Huang Tran, Vincent Vanhoucke, Quan Vuong, Ayzaan Wahid, Stefan Welker, Paul Wohlhart, Jialin Wu, Fei Xia, Ted Xiao, Peng Xu, Sichun Xu, Tianhe Yu, and Brianna Zitkovich. Rt-2: Vision-language-action models transfer web knowledge to robotic control. In [arXiv preprint arXiv:2307.15818](#), 2023.
- Qingwen Bu, Yanting Yang, Jisong Cai, Shenyuan Gao, Guanghui Ren, Maoqing Yao, Ping Luo, and Hongyang Li. Univla: Learning to act anywhere with task-centric latent actions. [arXiv preprint arXiv:2505.06111](#), 2025.
- Edresson Casanova, Ryan Langman, Paarth Neekhara, Shehzeen Hussain, Jason Li, Subhankar Ghosh, Ante Jukić, and Sang gil Lee. Low frame-rate speech codec: a codec designed for fast high-quality speech llm training and inference. [arXiv preprint arXiv:2409.12117](#), 2024.

- Xuelong Li Chenjia Bai, Huazhe Xu. Embodied-ai with large models: research and challenges. *SCIENTIA SINICA Informationis*, 2024.
- Cheng Chi, Zhenjia Xu, Siyuan Feng, Eric Cousineau, Yilun Du, Benjamin Burchfiel, Russ Tedrake, and Shuran Song. Diffusion policy: Visuomotor policy learning via action diffusion. *The International Journal of Robotics Research*, pp. 02783649241273668, 2023.
- Cheng Chi, Zhenjia Xu, Chuer Pan, Eric Cousineau, Benjamin Burchfiel, Siyuan Feng, Russ Tedrake, and Shuran Song. Universal manipulation interface: In-the-wild robot teaching without in-the-wild robots. *arXiv preprint arXiv:2402.10329*, 2024.
- Zibin Dong, Yicheng Liu, Yinchuan Li, Hang Zhao, and Jianye Hao. Conditioning matters: Training diffusion policies is faster than you think. In *The Thirty-ninth Annual Conference on Neural Information Processing Systems, NeurIPS*, 2025.
- Danny Driess, Fei Xia, Mehdi SM Sajjadi, Corey Lynch, Aakanksha Chowdhery, Brian Ichter, Ayzaan Wahid, Jonathan Tompson, Quan Vuong, Tianhe Yu, et al. Palm-e: An embodied multi-modal language model. *arXiv preprint arXiv:2303.03378*, 2023.
- Abhimanyu Dubey, Abhinav Jauhri, Abhinav Pandey, Abhishek Kadian, Ahmad Al-Dahle, Aiesha Letman, Akhil Mathur, Alan Schelten, Amy Yang, Angela Fan, et al. The llama 3 herd of models. *arXiv preprint arXiv:2407.21783*, 2024.
- Chongkai Gao, Zixuan Liu, Zhenghao Chi, Junshan Huang, Xin Fei, Yiwen Hou, Yuxuan Zhang, Yudi Lin, Zhirui Fang, Zeyu Jiang, and Lin Shao. Vla-os: Structuring and dissecting planning representations and paradigms in vision-language-action models. *arXiv preprint arXiv:2506.17561*, 2025. URL <https://arxiv.org/abs/2506.17561>.
- Yitian Gong, Luozhijie Jin, Ruifan Deng, Dong Zhang, Xin Zhang, Qinyuan Cheng, Zhaoye Fei, Shimin Li, and Xipeng Qiu. Xy-tokenizer: Mitigating the semantic-acoustic conflict in low-bitrate speech codecs. *arXiv preprint arXiv:2506.23325*, 2025.
- Asher J Hancock, Xindi Wu, Lihan Zha, Olga Russakovsky, and Anirudha Majumdar. Actions as language: Fine-tuning vlms into vlas without catastrophic forgetting. *arXiv preprint arXiv:2509.22195*, 2025.
- Physical Intelligence, Kevin Black, Noah Brown, James Darpinian, Karan Dhabalia, Danny Driess, Adnan Esmail, Michael Equi, Chelsea Finn, Niccolo Fusai, et al. pi0.5: a vision-language-action model with open-world generalization. *arXiv preprint arXiv:2504.16054*, 2025.
- Tao Jiang, Tianyuan Yuan, Yicheng Liu, Chenhao Lu, Jianning Cui, Xiao Liu, Shuiqi Cheng, Jiyang Gao, Huazhe Xu, and Hang Zhao. Galaxea open-world dataset and g0 dual-system vla model. *arXiv preprint arXiv:2509.00576*, 2025.
- Dmitry Kalashnikov, Alex Irpan, Peter Pastor, Julian Ibarz, Alexander Herzog, Eric Jang, Deirdre Quillen, Ethan Holly, Mrinal Kalakrishnan, Vincent Vanhoucke, et al. Scalable deep reinforcement learning for vision-based robotic manipulation. In *Conference on robot learning*, pp. 651–673. PMLR, 2018.
- Alexander Khazatsky, Karl Pertsch, Suraj Nair, Ashwin Balakrishna, Sudeep Dasari, Siddharth Karamcheti, Soroush Nasiriany, Mohan Kumar Srirama, Lawrence Yunliang Chen, Kirsty Ellis, et al. Droid: A large-scale in-the-wild robot manipulation dataset. *arXiv preprint arXiv:2403.12945*, 2024.
- Moo Jin Kim, Karl Pertsch, Siddharth Karamcheti, Ted Xiao, Ashwin Balakrishna, Suraj Nair, Rafael Rafailov, Ethan Foster, Grace Lam, Pannag Sanketi, et al. Openvla: An open-source vision-language-action model. *arXiv preprint arXiv:2406.09246*, 2024.
- Moo Jin Kim, Chelsea Finn, and Percy Liang. Fine-tuning vision-language-action models: Optimizing speed and success. *arXiv preprint arXiv:2502.19645*, 2025.
- Zineb Lahrichi, Gaëtan Hadjeres, Gael Richard, and Geoffroy Peeters. Qincodec: Neural audio compression with implicit neural codebooks. *arXiv preprint arXiv:2503.19597*, 2025.

- Doyup Lee, Chiheon Kim, Saehoon Kim, Minsu Cho, and Wook-Shin Han. Autoregressive image generation using residual quantization. In Proceedings of the IEEE/CVF Conference on Computer Vision and Pattern Recognition, CVPR, 2022.
- Bohan Li, Zhihan Li, Haoran Wang, Hanglei Zhang, Yiwei Guo, Hankun Wang, Xie Chen, and Kai Yu. Robust and efficient autoregressive speech synthesis with dynamic chunk-wise prediction policy. arXiv preprint arXiv:2506.22023, 2025.
- Xuanlin Li, Kyle Hsu, Jiayuan Gu, Karl Pertsch, Oier Mees, Homer Rich Walke, Chuyuan Fu, Ishikaa Lunawat, Isabel Sieh, Sean Kirmani, Sergey Levine, Jiajun Wu, Chelsea Finn, Hao Su, Quan Vuong, and Ted Xiao. Evaluating real-world robot manipulation policies in simulation. arXiv preprint arXiv:2405.05941, 2024a.
- Yanhong Li, Karen Livescu, and Jiawei Zhou. Chunk-distilled language modeling. arXiv preprint arXiv:2501.00343, 2024b.
- Bo Liu, Yifeng Zhu, Chongkai Gao, Yihao Feng, Qiang Liu, Yuke Zhu, and Peter Stone. Libero: Benchmarking knowledge transfer for lifelong robot learning. Advances in Neural Information Processing Systems, 36, 2024.
- Haotian Liu, Chunyuan Li, Qingyang Wu, and Yong Jae Lee. Visual instruction tuning. Advances in neural information processing systems, 36:34892–34916, 2023a.
- Shiwei Liu, Tianlong Chen, Xiaohan Chen, Xuxi Chen, Qiao Xiao, Boqian Wu, Tommi Kärkkäinen, Mykola Pechenizkiy, Decebal Constantin Mocanu, and Zhangyang Wang. More convnets in the 2020s: Scaling up kernels beyond 51x51 using sparsity. In The Eleventh International Conference on Learning Representations, ICLR, 2023b.
- Tao Liu, Ziyang Ma, Qi Chen, Feilong Chen, Shuai Fan, Xie Chen, and Kai Yu. Vqtalker: Towards multilingual talking avatars through facial motion tokenization. In Proceedings of the AAAI Conference on Artificial Intelligence, AAAI, 2025.
- Van Khoa Nguyen, Yoann Boget, Frantzeska Lavda, and Alexandros Kalousis. GLAD: Improving latent graph generative modeling with simple quantization. In ICML 2024 Workshop on Structured Probabilistic Inference and Generative Modeling, ICML, 2024.
- Julian D Parker, Anton Smirnov, Jordi Pons, CJ Carr, Zack Zukowski, Zach Evans, and Xubo Liu. Scaling transformers for low-bitrate high-quality speech coding. arXiv preprint arXiv:2411.19842, 2024.
- Julian D Parker, Anton Smirnov, Jordi Pons, CJ Carr, Zack Zukowski, Zach Evans, and Xubo Liu. Scaling transformers for low-bitrate high-quality speech coding. In The Thirteenth International Conference on Learning Representations, ICLR, 2025.
- Karl Pertsch, Kyle Stachowicz, Brian Ichter, Danny Driess, Suraj Nair, Quan Vuong, Oier Mees, Chelsea Finn, and Sergey Levine. Fast: Efficient action tokenization for vision-language-action models. arXiv preprint arXiv:2501.09747, 2025.
- Delin Qu, Haoming Song, Qizhi Chen, Yuanqi Yao, Xinyi Ye, Yan Ding, Zhigang Wang, JiaYuan Gu, Bin Zhao, Dong Wang, et al. Spatialvla: Exploring spatial representations for visual-language-action model. arXiv preprint arXiv:2501.15830, 2025.
- Alec Radford, Jeffrey Wu, Rewon Child, David Luan, Dario Amodei, Ilya Sutskever, et al. Language models are unsupervised multitask learners. OpenAI blog, 1(8):9, 2019.
- Samir Sadok, Simon Leglaive, and Renaud Séguier. A vector quantized masked autoencoder for audiovisual speech emotion recognition. Computer Vision and Image Understanding, 2025.
- Kyle Sargent, Kyle Hsu, Justin Johnson, Li Fei-Fei, and Jiajun Wu. Flow to the mode: Mode-seeking diffusion autoencoders for state-of-the-art image tokenization. In arXiv preprint arXiv:2503.11056, 2025.

- Andreas Steiner, André Susano Pinto, Michael Tschannen, Daniel Keysers, Xiao Wang, Yonatan Bitton, Alexey Gritsenko, Matthias Minderer, Anthony Sherbondy, Shangbang Long, et al. Paligemma 2: A family of versatile vlms for transfer. [arXiv preprint arXiv:2412.03555](#), 2024.
- Tianxiang Sun, Xiaotian Zhang, Zhengfu He, Peng Li, Qinyuan Cheng, Xiangyang Liu, Hang Yan, Yunfan Shao, Qiong Tang, Shiduo Zhang, Xingjian Zhao, Ke Chen, Yining Zheng, Zhejian Zhou, Ruixiao Li, Jun Zhan, Yunhua Zhou, Linyang Li, Xiaogui Yang, Lingling Wu, Zhangyue Yin, Xuanjing Huang, Yu-Gang Jiang, and Xipeng Qiu. Moss: An open conversational large language model. *Machine Intelligence Research*, 2024. ISSN 2731-5398. doi: 10.1007/s11633-024-1502-8. URL <https://doi.org/10.1007/s11633-024-1502-8>.
- Anni Tang, Tianyu He, Junliang Guo, Xinle Cheng, Li Song, and Jiang Bian. Vidtok: A versatile and open-source video tokenizer. In [arXiv preprint arXiv:2412.13061](#), 2024.
- Galaxea Team. Galaxea manipulation simulator. 2025.
- Octo Model Team, Dibya Ghosh, Homer Walke, Karl Pertsch, Kevin Black, Oier Mees, Sudeep Dasari, Joey Hejna, Tobias Kreiman, Charles Xu, et al. Octo: An open-source generalist robot policy. [arXiv preprint arXiv:2405.12213](#), 2024.
- Keyu Tian, Yi Jiang, Zehuan Yuan, BINGYUE PENG, and Liwei Wang. Visual autoregressive modeling: Scalable image generation via next-scale prediction. In [The Thirty-eighth Annual Conference on Neural Information Processing Systems, NeurIPS](#), 2024.
- Aaron Van Den Oord, Oriol Vinyals, et al. Neural discrete representation learning. [Advances in neural information processing systems](#), 30, 2017.
- Homer Rich Walke, Kevin Black, Tony Z Zhao, Quan Vuong, Chongyi Zheng, Philippe Hansen-Estruch, Andre Wang He, Vivek Myers, Moo Jin Kim, Max Du, et al. Bridgedata v2: A dataset for robot learning at scale. In [Conference on Robot Learning](#), pp. 1723–1736. PMLR, 2023.
- Junke Wang, Yi Jiang, Zehuan Yuan, BINGYUE PENG, Zuxuan Wu, and Yu-Gang Jiang. Omnitokenizer: A joint image-video tokenizer for visual generation. In [The Thirty-eighth Annual Conference on Neural Information Processing Systems, NeurIPS](#), 2024a.
- Limei Wang, Kaveh Hassani, Si Zhang, Dongqi Fu, Baichuan Yuan, Weilin Cong, Zhigang Hua, Hao Wu, Ning Yao, and Bo Long. Learning graph quantized tokenizers. In [ICLR](#), 2025a.
- Weiyun Wang, Zhangwei Gao, Lixin Gu, Hengjun Pu, Long Cui, Xingguang Wei, Zhaoyang Liu, Linglin Jing, Shenglong Ye, Jie Shao, et al. Internvl3. 5: Advancing open-source multimodal models in versatility, reasoning, and efficiency. [arXiv preprint arXiv:2508.18265](#), 2025b.
- Xiaofeng Wang, Zheng Zhu, Guan Huang, Boyuan Wang, Xinze Chen, and Jiwen Lu. World-dreamer: Towards general world models for video generation via predicting masked tokens. [arXiv preprint arXiv:2401.09985](#), 2024b.
- Yating Wang, Haoyi Zhu, Mingyu Liu, Jiange Yang, Hao-Shu Fang, and Tong He. Vq-vla: Improving vision-language-action models via scaling vector-quantized action tokenizers. [arXiv preprint arXiv:2507.01016](#), 2025c.
- Qwen Team: An Yang, Baosong Yang, Beichen Zhang, Binyuan Hui, Bo Zheng, Bowen Yu, Chengyuan Li, Dayiheng Liu, Fei Huang, Haoran Wei, Huan Lin, Jian Yang, Jianhong Tu, Jianwei Zhang, Jianxin Yang, Jiaxi Yang, Jingren Zhou, Junyang Lin, Kai Dang, Keming Lu, Keqin Bao, Kexin Yang, Le Yu, Mei Li, Mingfeng Xue, Pei Zhang, Qin Zhu, Rui Men, Runji Lin, Tianhao Li, Tianyi Tang, Tingyu Xia, Xingzhang Ren, Xuancheng Ren, Yang Fan, Yang Su, Yichang Zhang, Yu Wan, Yuqiong Liu, Zeyu Cui, Zhenru Zhang, and Zihan Qiu. Qwen2.5 technical report. [arXiv preprint arXiv:2412.15115](#), 2025a.
- Shuai Yang, Wei Huang, Ruihang Chu, Yicheng Xiao, Yuyang Zhao, Xianbang Wang, Muyang Li, Enze Xie, Yingcong Chen, Yao Lu, et al. Longlive: Real-time interactive long video generation. [arXiv preprint arXiv:2509.22622](#), 2025b.

- Lijun Yu, Yong Cheng, Kihyuk Sohn, José Lezama, Han Zhang, Huiwen Chang, Alexander G Hauptmann, Ming-Hsuan Yang, Yuan Hao, Irfan Essa, and Lu Jiang. MAGVIT: Masked generative video transformer. In Proceedings of the IEEE/CVF Conference on Computer Vision and Pattern Recognition, CVPR, 2023.
- Qihang Yu, Mark Weber, Xueqing Deng, Xiaohui Shen, Daniel Cremers, and Liang-Chieh Chen. An image is worth 32 tokens for reconstruction and generation. In The Thirty-eighth Annual Conference on Neural Information Processing Systems, NeurIPS, 2024.
- Long Zeng, Jianxiang Yu, Jiapeng Zhu, Qingsong Zhong, and Xiang Li. Hierarchical vector quantized graph autoencoder with annealing-based code selection. In THE WEB CONFERENCE 2025, WWW, 2025.
- Linwei Zhai, Han Ding, Cui Zhao, fei wang, Ge Wang, Wang Zhi, and Wei Xi. L3ac: Towards a lightweight and lossless audio codec. arXiv preprint arXiv:2504.04949, 2025.
- Shiduo Zhang, Zhe Xu, Peiju Liu, Xiaopeng Yu, Yuan Li, Qinghui Gao, Zhaoye Fei, Zhangyue Yin, Zuxuan Wu, Yu-Gang Jiang, et al. Vlabench: A large-scale benchmark for language-conditioned robotics manipulation with long-horizon reasoning tasks. arXiv preprint arXiv:2412.18194, 2024.
- Siyang Zhang and Ser-Nam Lim. Towards chunk-wise generation for long videos. arXiv preprint arXiv:2411.18668, 2024.
- Xin Zhang, Dong Zhang, Shimin Li, Yaqian Zhou, and Xipeng Qiu. Speeche tokenizer: Unified speech tokenizer for speech large language models. arXiv preprint arXiv:2308.16692, 2023.
- Xinyu Zhang, Yuhan Liu, Haonan Chang, Liam Schramm, and Abdeslam Boularias. Autoregressive action sequence learning for robotic manipulation. IEEE Robotics and Automation Letters, 2025.
- Tony Z Zhao, Vikash Kumar, Sergey Levine, and Chelsea Finn. Learning fine-grained bimanual manipulation with low-cost hardware. arXiv preprint arXiv:2304.13705, 2023.
- Yue Zhao, Yuanjun Xiong, and Philipp Krähenbühl. Image and video tokenization with binary spherical quantization. arXiv preprint arXiv:2406.07548, 2024.
- Hongyi Zhou, Weiran Liao, Xi Huang, Yucheng Tang, Fabian Otto, Xiaogang Jia, Xinkai Jiang, Simon Hilber, Ge Li, Qian Wang, et al. Beast: Efficient tokenization of b-splines encoded action sequences for imitation learning. arXiv preprint arXiv:2506.06072, 2025.

A APPENDIX

A.1 DETAILED EVALUATION SETUPS.

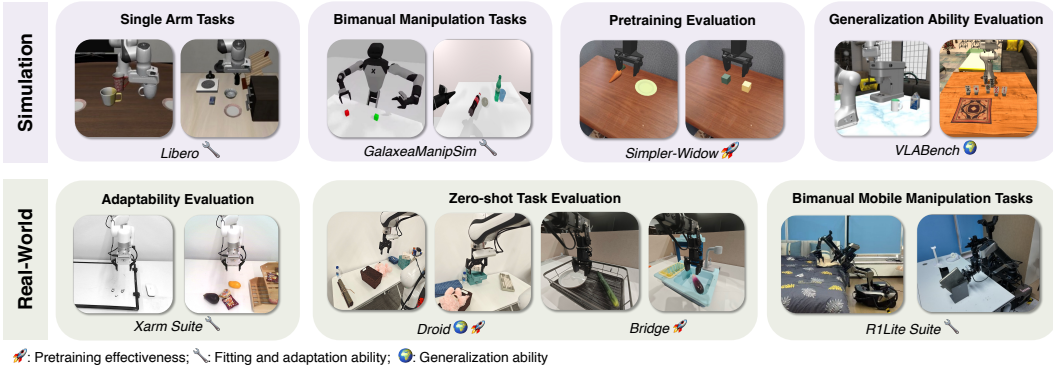


Figure 11: **Experiment setups.** Diverse embodiments, scenes, and tasks for assessing multiple capability dimensions (marked by emojis).

Benchmarks&Evaluation Details. We evaluate FASTerVLA across multiple dimensions, including out-of-the-box performance after pre-training, adaptability through fine-tuning on downstream tasks, and generalization ability under visual and language perturbations as well as in zero-shot settings. We adopt a variety of benchmark suites with distinct focuses, encompassing diverse robot embodiments and task distributions. For a fair ablation, we make every effort to use the same training settings as the other baselines. The evaluation setup below lists our training recipes and evaluation protocols.

- **Libero** (Liu et al., 2024) includes four task suites—Spatial, Object, Goal, and Long—with a total of 40 tasks, each containing 50 examples. This benchmark is particularly suitable for assessing both the models’ capacity to fit the data and their adaptability to downstream tasks. To further compare the advantages of different model architectures, we evaluate two settings: models pre-trained and then fine-tuned on Libero, and models trained directly on Libero via imitation learning from scratch. We train a single policy across all four task suites. The results are reported in Table 1 and Figure 4, respectively. Following the official π_0 fine-tuning recipe, we train the model under a multi-task joint training setting for 30k steps, using a global batch size of 32, with image augmentation disabled, on 8 H100 GPUs. This model leverages FasterVQ(S), as listed in Table 3.
- **Simpler-widow** (Li et al., 2024a) serves as a benchmark for assessing the pre-training performance of VLAs. Table 1 reports the evaluation results of models trained from scratch on Bridge dataset (Walke et al., 2023). The models were trained for 4 epochs with image augmentation enabled, using a global batch size of 128 across 8 H100 GPUs. FASTerVLA utilizes FasterVQ(S), as described in Table 3. Unlike the default Simpler settings, which evaluate 24 trials for each task, we evaluate each task for 120 trials to mitigate the noise introduced by the high variance in zero-shot evaluation.
- **VLABench** (Zhang et al., 2024) is a benchmark focusing on the generalization capabilities of VLAs. We finetune our models on 10 tasks from VLABench, with a total of 5,000 examples. VLABench offers rigorously controlled evaluations across multiple dimensions, including complex instruction following, visual disturbances, language grounding, and commonsense transfer. We fine-tune the pretrained models— π_0 , π_0 -FAST, and FasterVLA—on 5,000 diverse episodes covering 10 tasks from VLABench. All models were trained for 30k steps with a global batch size of 32, no image augmentation, and executed on 8 H100 GPUs. The tokenizer used in FASTer was trained separately on the VLABench primitive dataset.
- **GalaxeaManipSim** (Team, 2025). Using this simulator, we evaluate the model on seven dual-arm tasks—BlockHammerBeat, BlocksStackEasy, ContainerPlace, DiverseBottlesPick, DualBottlesPickHard, EmptyCupPlace, and ShoePlace—with a total of 7,000 examples. The embodiments used in the simulator are R1 and R1Lite. We chose π_0 , π_0 -FAST as the baselines. All models were trained for 4 epochs with image augmentation enabled, using a global batch size of 128 across 8 H20 GPUs. We use three camera views, including the head camera and the left and right wrist

Table 3: Overview of data mixtures used for training FASTERVQ.

Mixture Name	Datasets	Ratio	Application
Galaxea	Galaxea Open Dataset (Jiang et al., 2025)	1.0	Used for RILite Evaluation.
Droid Mixture	Droid (Joint Velocity) (Khazatsky et al., 2024)	1.0	Used for Droid evaluation.
FASTer(S)	Libero (Liu et al., 2024)	5.0	Used for libero, simpler and widow evaluation.
	Bridge (Walke et al., 2023)	1.0	
FASTer(L)	Libero (Liu et al., 2024)	5.0	Used for Xarm finetuning and tokenizer scaling analysis.
	Bridge (Walke et al., 2023)	1.0	
	Kuka (Kalashnikov et al., 2018)	1.0	
	Fractal (Brohan et al., 2023)	1.0	
	Droid(EFF) (Khazatsky et al., 2024)	1.0	
FASTer(XL)	Libero (Liu et al., 2024)	5.0	Used for tokenizer scaling and action representation analysis.
	Bridge (Walke et al., 2023)	1.0	
	Kuka (Kalashnikov et al., 2018)	1.0	
	Fractal (Brohan et al., 2023)	1.0	
	Droid(EFF) (Khazatsky et al., 2024)	1.0	
	Droid(Joint Velocity) (Khazatsky et al., 2024)	1.0	
	Galaxea Open Dataset (Jiang et al., 2025)	1.0	

cameras. The FASTERVQ was trained on the Galaxea Open Dataset (Jiang et al., 2025) without post-training.

- **Xarm Suite** features an XArm dataset that covers five tasks, with 500 real-world episodes. These tasks involve flexible object manipulation, multi-goal selection, and long-horizon planning. The tasks include: board wiping, poker choosing, fruit placing, object managing, and towel folding. We conducted joint training on 500 samples across these tasks, using a total batch size of 128 with image augmentation, for 30k training steps. We employ FASTERVQ(L) in this model, as shown in Table 3.
- **RILite Suite** includes three real-world tasks to evaluate our system: two desktop-level tasks—picking cubes and table bussing—and one whole-body control task, making the bed. The dataset sizes are 200 demonstrations for picking cubes, 200 demonstrations for desk organization, and 1,000 demonstrations for bed making. We chose π_0 , π_0 -FAST as the baselines. We train our model and baselines for 8 epochs, using a global batch size of 256 across 64 H20 GPU. The FASTERVQ was trained on the Galaxea Open Dataset (Jiang et al., 2025) without post-training.
- **Bridge** (Walke et al., 2023) is a large-scale manipulation dataset with over 60k trajectories. Following its hardware setup, we use Widow250s for zero-shot evaluation after pre-training. The checkpoints used in this experiment are the same as those in Simpler.
- **Droid** (Khazatsky et al., 2024) contains over 90k real-world robotics trajectories. To ensure consistent evaluation, we follow its hardware setup and evaluate models in a zero-shot setting after pre-training. Following (Intelligence et al., 2025), we train on the Droid dataset for 3 epochs using 64 H200 GPUs, with a per-GPU batch size of 16, resulting in a total batch size of 1024, and adopt joint-velocity control.

A.2 IMPLEMENTATION DETAILS

Data Mixture. In the experiments of Section 4, we trained FASTERVQ with different data mixtures. We report the detailed mixtures in Table 3.

FASTerVQ. We trained all policies using AdamW with a learning rate of 1×10^{-4} , weight decay 0.1, and $(\beta_1, \beta_2) = (0.9, 0.95)$. The learning rate followed a cosine decay schedule with 1,000 warmup steps. Gradients were clipped at norm 1.0, and training used mixed precision (bfloat16). The single-arm policy (8M parameters) was trained with a batch size of 512 sequences of length 21 tokens, whereas the full-body policy (13M parameters) was trained with a batch size of 2048 sequences of the same length. All models were trained on $8 \times$ H100 GPUs, and training converged within 300k steps. We set the codebook size to $K = 4096$, the latent dimension to $d = 128$, and the commitment cost to $\beta = 0.25$. The detailed hyperparameters and settings used for each evaluation environment are provided in Table 4.

FASTerVLA. We trained the VLA using AdamW with a learning rate of 2.5×10^{-5} and weight decay 1×10^{-10} . The learning rate followed a cosine decay schedule with 1,000 warmup steps, and training used mixed precision (bfloat16). The attention dropout was set to 0.0. For inference,

Table 4: Detailed Hyperparameter Configuration for FASTerVQ and BAR.

Suite	Embodiment	Action DoF	BAR block size	Action chunk size	C_a	C_h	Number of codebook
Libero	Franka	7	7	20	7	1	3
Simpler	Widow250s	6	7	10	7	1	3
VLABench	Franka	7	7	10	7	1	3
GalaxeaManipSim	R1, R1Lite	14	7	32	14	2	3
Xarm Suite	XArm	7	7	20	7	1	3
R1Lite Suite	R1Lite	21	7	32	21	2	3
Bridge	Widow250	6	7	10	7	1	3
Droid	Franka	7	7	20	7	1	3

Table 5: Inference time across environments and models, measured on an NVIDIA GeForce RTX 5090 using PyTorch.

Environment	Model	FASTer	pi0	FAST
	LIBERO (ms)		112	176
R1Lite-WBC (ms)		237	225	1,100–3,000

we employed top- k sampling ($k = 50$) with temperature 0.8. Block-wise autoregressive decoding was used, with a block size of 8 for WBC and bimanual tasks, and 7 for the single-arm setting. The hyperparameters used for action tokenization and BAR are listed in Table 4. We set the conditioning window to 1 step, and the final actions were clipped to the range $[-1, 1]$.

A.3 ABLATION STUDY

FASTerVQ Ablations. As shown in Table 6, FASTerVQ exhibits clear performance trends across the three ablated dimensions. The TAAE tokenizer delivers the strongest reconstruction fidelity, reflected by the lowest ℓ_1 loss, and also reaches the highest success rate, surpassing both the CNN and Transformer variants. Increasing the codebook size improves representation capacity up to 4096 entries, at which point success rate and utilization peak before degrading at 8192, indicating the onset of codebook collapse. Finally, residual quantization yields the most stable gains with two to three residual layers, whereas deeper stacks introduce diminishing returns or mild instability. Together, these observations support the final choice adopted in our design: a TAAE tokenizer coupled with a 4096-entry codebook and three residual codebooks, which jointly provide the most favorable balance between reconstruction quality and policy success rate.

FASTerVLA Ablations. We examine two essential components of VLA: the action expert (AE) responsible for action tokenization, and the block-wise autoregressive (BAR) decoding mechanism. Table 7 reveals that on **libero**, AE consistently enhances SR relative to the no-AE baseline, with pretraining providing the most pronounced gain (97.9 vs. 95.5). On **simpler-widow**, AE trained from scratch collapses (23.6), suggesting that gradients from the VLM offer only a faint signal for learning a high-quality action tokenizer. Pretraining therefore becomes indispensable, lifting SR to 87.9. These observations naturally motivate a two-stage training scheme: first pretrain AE within the VLM, then fine-tune jointly with partial freezing. This schedule accelerates convergence and markedly stabilizes optimization. For decoding, BAR substantially improves both accuracy and efficiency: SR rises from 95.5 to 96.7, while latency is reduced by more than $2\times$ (323,ms to 140,ms). When BAR is combined with AE, SR further increases to 97.7 at the same low latency, offering the most harmonious balance between precision and speed.

We also ablate different BAR block sizes. Our intuition is that BAR becomes effective when the action-token sequence exhibits a relatively stable length and when meaningful correlations are preserved across tokens. Under such conditions, BAR can be applied directly and remains reliable. We evaluate multiple BAR block sizes using the same FASTerVQ configuration with an action code length of 42. As shown in Section A.3, performance remains stable as long as the block size lies within a reasonable multiple of the action-dimension code length. When the block size matches this code length, the result is the strongest. Empirically, these findings echo our design intuition: BAR integrates seamlessly with FASTerVQ because FASTerVQ preserves the latent structure of action chunks, allowing BAR to exploit this structure for coherent block-wise generation.

Table 6: **Ablation on FASTERVQ** policy success rate in libero simulator (SR, %) and ℓ_1 loss (lower is better);

Arch.	(a) Tokenizer		(b) Codebook Size			(c) Residual	
	SR	ℓ_1	Size	SR	utilization	#Res.	SR
CNN	96.2	0.0027	512	95.4	100	1	93.4
Transf.	95.3	0.0036	1024	93.2	100	2	95.5
TAAE	97.9	0.0021	4096	97.9	99.6	3	97.9
-	-	-	8192	96.3	95.1	8	96.6

Table 7: Ablation studies of FASTER. Left: ablation study of the action expert (AE) on **libero**; Middle: AE on **simpler-widow**; Right: BAR decoding. “Pretrain” indicates whether the model is initialized from a checkpoint pretrained on robotics datasets; others without this label are all initialized from such pretrained checkpoints.

libero (AE)		simpler-widow (AE)		bar decoding		
Variant	SR \uparrow	Variant	SR \uparrow	Decoding strategy	SR \uparrow	Latency (ms) \downarrow
No AE	95.5	No AE	75.6	Token-wise (AR)	95.5	323
AE (no pretrain)	94.8	AE (no pretrain)	23.6	Block-wise	96.7	140
AE (with pretrain)	97.9	AE (with pretrain)	87.9	Block-wise + AE (FASTer)	97.7	140

A.4 DETAILED RESULTS OF DIFFERENT VLM BACKBONES

To evaluate the effectiveness and adaptability of our framework, we conducted comprehensive experiments on the Libero benchmark. We selected several popular VLM backbones: Paligemma-3B (Steiner et al., 2024), InternVL3.5-2B (Wang et al., 2025b), and various sizes of Qwen2.5 (0.5B, 1.5B, 3B) (Yang et al., 2025a). For Paligemma and InternVL, we utilized their original VLM checkpoints. For the Qwen2.5 models, we adopted the VLM checkpoints provided by (Gao et al., 2025), which fine-tuned the base LLM with a vision tower and projector on the LLaVa v1.5 dataset (Liu et al., 2023a). All these backbones were subsequently trained from scratch on the Libero benchmark. We compared their performance against the baseline FAST tokenizer.

The detailed results in Table 9 demonstrate that our framework achieves consistent and significant performance improvements across all tested model architectures and parameter scales. Notably, while Paligemma-3B delivered the strongest performance among all models using the FAST tokenizer (93.50 Average), our framework was able to unlock the latent potential of other VLMs. For instance, InternVL3.5-2B, which had the weakest performance with the FAST tokenizer (79.35 Average), was elevated to become the top-performing model overall (96.65 Average) when paired with our tokenizer. This is particularly significant given that InternVL 3.5 is inherently competitive on embodied benchmarks, indicating that our method successfully unleashes its latent potential for action generation. This remarkable turnaround not only proves the effectiveness of our framework but also highlights its broad adaptability and its ability to fully harness the capabilities of diverse VLM backbones.

Table 9: Detailed performance of different VLM backbones on Libero

Model	Tokenizer	Spatial	Object	Goal	Long	Average
Qwen2.5-0.5B	FAST	92.60	95.80	70.00	78.20	84.15
	Ours	90.40	99.00	71.60	87.00	87.00 (\uparrow 2.85)
Qwen2.5-1.5B	FAST	96.00	92.80	87.20	85.80	90.45
	Ours	94.40	97.80	92.00	84.80	92.25 (\uparrow 1.80)
Qwen2.5-3B	FAST	97.80	93.80	90.20	83.40	91.30
	Ours	96.40	99.40	92.00	94.00	95.45 (\uparrow 4.15)
InternVL3.5-2B	FAST	92.60	95.20	77.20	52.40	79.35
	Ours	97.80	98.60	97.20	93.00	96.65 (\uparrow 17.30)
Paligemma2-3B	FAST	93.40	98.80	95.00	86.80	93.50
	Ours	96.60	98.00	95.20	89.40	94.80 (\uparrow 1.30)

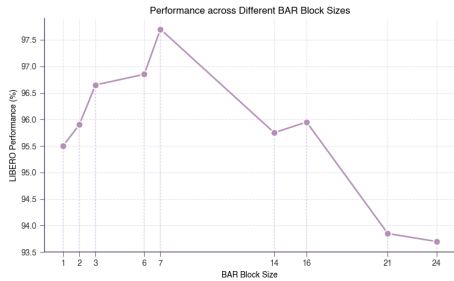


Figure 12: Different BAR block sizes, including irregular granularity, and their performance on the LIBERO environment.

A.5 QUALITATIVE ANALYSIS OF THE TOKENIZER

To evaluate the effectiveness of different action tokenizers, we conduct a qualitative and quantitative analysis covering reconstruction fidelity, token utilization, and generalization across datasets and embodiments.

VQ Settings. The following VQ tokenizer configurations are used in our reconstruction visualizations and token usage analyses, covering prior baselines and our proposed model.

- **MiniVLA’s VQ** (Belkhale & Sadigh, 2024) uses residual vector quantization to encode action chunks into sequences of codeword indices, with optional extra tokens in the vocabulary. For our experiments, we use the official VQ weights released by the authors: one trained on Libero and the other on Bridge V2 Dataset.
- **VQ-VLA’s VQ** (Wang et al., 2025c) replaces OpenVLA’s simple binning with a residual VQ tokenizer that encodes action sequences into discrete codeword indices using hierarchical quantization. In our experiments, we pretrain the VQ from scratch using the VQ-VLA training framework and code, on a 1:1 mixture of LIBERO and BRIDGE with a single H200 GPU (batch size 1024, 800k steps, learning rate 5e-5).
- **Fast+** (Pertsch et al., 2025) is the universal action tokenizer of Fast, trained on one million real-world robot trajectories.
- **FasterVQ** is our proposed VQ, with the training data mixtures summarized in Table 3.

Action Reconstruction Visualization. We qualitatively assess the learned VQ models by visualizing normalized action sequence reconstructions from Libero, Bridge, XArm, and Widow (Figure 14), comparing MiniVLA, VQ-VLA, Fast+, and Faster in terms of fidelity and generalization. In each plot, the red line denotes the ground-truth trajectory, the green line denotes the reconstruction, and the shaded red region denotes the error band with a tolerance of 0.01. Note that the green horizontal line in the figure appears due to clipping in the normalization at the 99th percentile bound.

On in-domain datasets such as Libero and Bridge, most predicted chunks remain within the 0.01 error band, indicating reasonable fidelity. However, their performance degrades notably on out-of-domain datasets like XArm and Widow, where a larger fraction of predictions exceed the tolerance. Reconstructions from MiniVLA and VQ-VLA exhibit more frequent spiky artifacts. Fast+ and FasterVQ preserve stable reconstructions across both seen and unseen domains, with most chunks remaining within the error band and some trajectories exhibiting nearly exact overlap with the ground truth.

Token Activation Statistics. Table 10 compares codebook size, active tokens, and usage frequency across VQ tokenizers. Small codebooks (VQ-VLA, MiniVLA) are fully activated. Fast+ underutilizes its larger vocabulary. In contrast, FasterVQ effectively harnesses a much larger codebook, activating thousands of tokens with a meaningful subset above frequency thresholds. This avoids token collapse and provides richer, more fine-grained representations.

Detailed VRR Evaluation Results. Figure 5 in Section 4 presents the average VRR values across four datasets for the FASTER, Fast, MiniVLA-VQ, and VQ-VLA-VQ tokenizers under different θ scales. Figure 13 provides a more detailed view, showing the VRR scores for each dataset at the three θ thresholds corresponding to meaningful physical error levels. Across multiple θ scales, the

Metric	Fast	Fast+	FASTer
$N_{\text{vocab}} \uparrow$	2048	2048	4096
$Usage [\%] \uparrow$	48.39	57.37	100.0
$N_{\text{active}} (\sigma = 10^{-2}) \downarrow$	8	16	3
$F_{\text{max}} [\%] \downarrow$	9.63	1.82	1.35
$Entropy_{\text{norm}} \uparrow$	0.69	0.77	0.91

Table 8: Comparison of vocabulary distributions of different tokenizers on the Bridge.

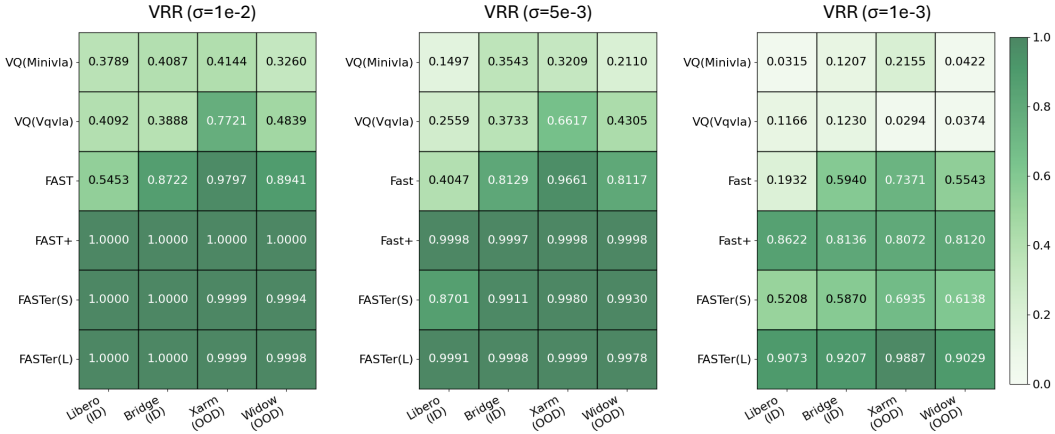


Figure 13: Heatmap for detailed VRR of different tokenizers across ID and OOD datasets.

Table 10: Token activation statistics on Bridge and XArm-mixture. Columns show codebook size, active tokens, and counts of tokens exceeding the 10^{-3} and 2×10^{-2} thresholds.

Tokenizer	Bridge				XArm			
	CB	Act.	$> 1e^{-3}$	$> 2e^{-2}$	CB	Act.	$> 1e^{-3}$	$> 2e^{-2}$
VQ-VLA-vq (800k)	256	256	–	1	256	256	–	1
MiniVLA-vq-bridge	256	256	–	1	256	256	–	1
Fast+	2048	1175	200	–	2048	1067	216	–
FasterVQ	4096	4096	162	–	4096	4096	38	–

results show that previous VQ-based methods exhibit extremely poor reconstruction performance, which implies that the VLA backbone is effectively learning a biased supervision signal. Under the same amount of training data, FASTER(S) significantly outperforms Fast. Moreover, even when Fast+ is trained with substantially more data than FASTER(L), FASTER(L) still surpasses Fast+ in reconstruction quality.

A.6 USE OF LLM

We utilized LLMs as a writing assistance tool during the preparation of this manuscript. The use of LLMs was strictly limited to polishing the text, which included improving grammar, refining sentence structure, and enhancing overall clarity and readability. The core research concepts, methodologies, and conclusions were developed entirely by the authors.

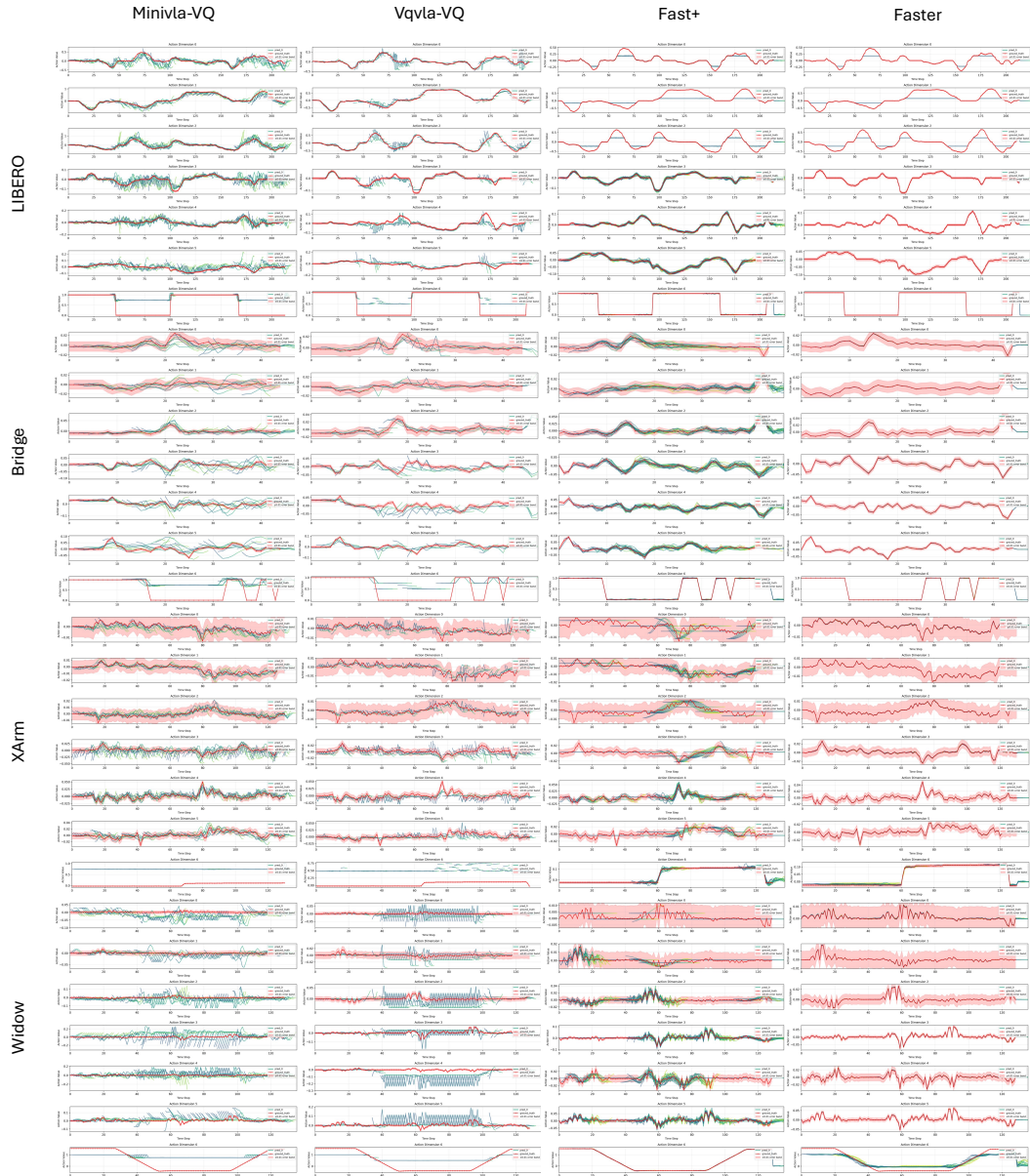


Figure 14: Visualization of action reconstruction results from MiniVLA, VQ-VLA, Fast+, and FasterVQ on representative trajectories from the Libero, Bridge, XArm, and Widow datasets.

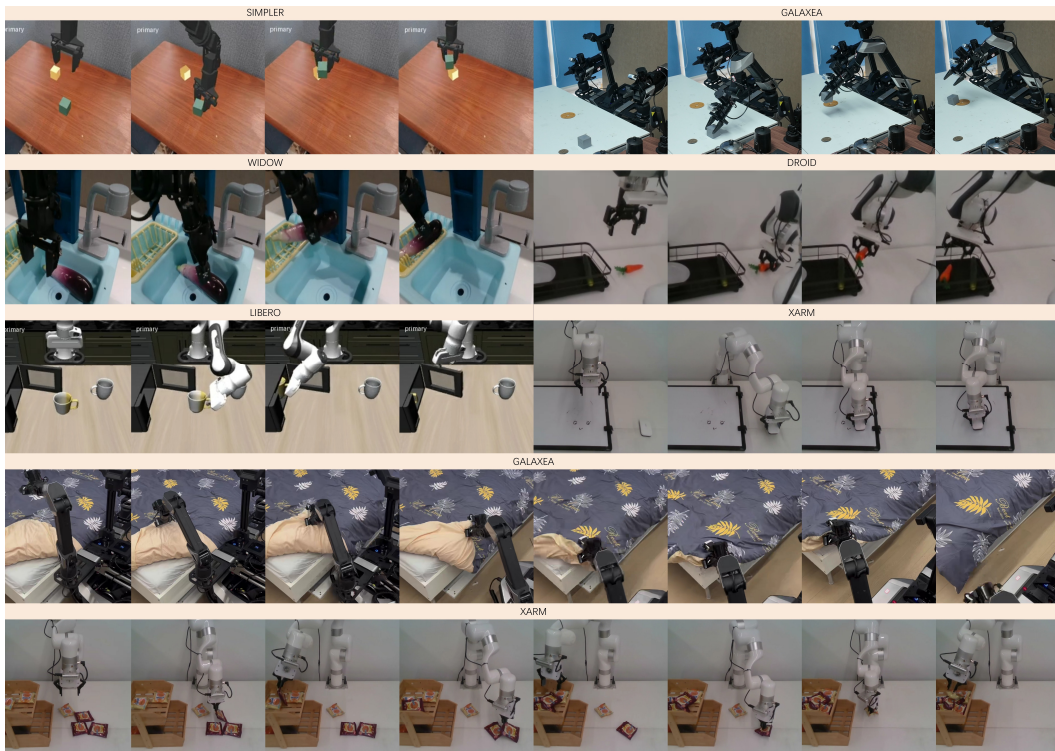


Figure 15: Visualization of our evaluation tasks.